Sensors & Diagnostics

PAPER

View Article Online
View Journal | View Issue

Cite this: *Sens. Diagn.*, 2024, **3**, 295

Artificial light-harvesting nanoparticles based on a tripodal fluorescence sensor mediated by multiple luminescence mechanisms†

Zhiying Wu, Qiaona Zhang, Dengli Chen and Tangxin Xiao *

It is highly desirable to precisely control the luminescence properties of organic molecules through the combination of multiple fluorescence mechanisms. In this work, we designed and synthesized a tripodal sensor molecule **G**, which contains three tetraphenylethylene (TPE) groups and three Schiff base groups. The **G** molecules can form nanoparticles in H_2O/THF mixed solvent (f_w = 90%) through the reprecipitation method. Moreover, by co-precipitation with an energy acceptor dye **NDI**, efficient artificial light harvesting nanoparticles (**G–NDI** NPs) could be obtained. As a result, a combination of three fluorescence mechanisms was introduced into this binary system: excited-state intramolecular proton-transfer (ESIPT) based on Schiff base groups, aggregation-induced emission (AIE) based on TPE groups, and Förster resonance energy transfer (FRET) between the donor and acceptor. At a relatively high donor/acceptor ratio (200/1), the antenna effect can reach 11.4 and the energy transfer efficiency can reach 22.0%. Furthermore, these assembled NPs were successfully used in the detection of Fe^{3+} and Cu^{2+} ions and showed good probing abilities with large Stokes shifts and red fluorescence quenching phenomena. This study will further inspire the development of multi-color luminescent materials by controlling multiple mechanisms and show great potentials in chemical sensing, bioimaging, and photoluminescent devices.

Received 1st November 2023,
Accepted 15th December 2023

DOI: 10.1039/d3sd00297g

rsc.li/sensors

Introduction

Natural photosynthesis is vital for all living things on the Earth. The initial process of photosynthesis is the harvesting of sunlight through a large number of antenna chromophores.[1,2] The absorbed energy was stepwise transferred in chlorophyll and eventually reaches the reaction center. Inspired by nature, many artificial light-harvesting systems (LHSs)[3–9] have been reported in recent years for different applications, such as photocatalysis,[10–23] bio-imaging,[24–26] information encryption[27–29] and light-emitting devices.[30–33] These systems are often nanoparticles (NPs) dispersed in aqueous media to meet the requirement of green production. Strategies for preparing such NPs generally include self-assembly,[34–37] micro-emulsion,[38–43] reprecipitation[44,45] *etc.* For example, Wang and co-workers constructed artificial light-harvesting NPs based on the self-assembly of water-soluble pillar[6]arene.[46] Yang and co-workers pioneered the fabrication of light-harvesting NPs through a micro-emulsion method.[47] Acharyya and co-workers reported light-harvesting NPs with cascade energy transfer built in 90% water-acetone solution.[48] However, the organic donor fluorophores used in these NPs often lack further functionality, such as sensing capabilities, hindering their application in chemical/biosensing fields. Therefore, it is highly desirable to create functional light-harvesting NPs based on multi-functional donor molecules in an efficient manner for chemical sensing.

To enable the NPs to be highly emissive, aggregation-induce emission (AIE)[49–53] fluorophores are reasonably chosen owing to their high luminescence efficiency in a confined micro-environment. Actually, light-harvesting NPs based on the AIE fluorophore have received considerable attention recently.[8] To avoid self-absorption and achieve large Stokes shift in organic fluorescent molecules, the excited-state intramolecular proton-transfer (ESIPT) mechanism is often adopted.[54–56] ESIPT is a process in which excited molecules with intramolecular hydrogen bonds relax their energy through tautomerization by proton transfer. The integration of AIE and ESIPT in one organic molecule can be realized straightforwardly by molecular structure modification, affording highly fluorescent NPs with a large Stokes shift. By introducing proper acceptor dyes into the NPs, Förster resonance energy transfer (FRET) could be further occured.[57–59] Based on the idea of this AIE–ESIPT–FRET triple fluorescence mechanism, we previously reported a spirocyclic bridged double tetraphenylethylene (TPE) derivative to

School of Petrochemical Engineering, Changzhou University, Changzhou 213164, China. E-mail: xiaotangxin@cczu.edu.cn

† Electronic supplementary information (ESI) available. See DOI: https://doi.org/10.1039/d3sd00297g

achieve the construction of a LHS and the recognition of metal ions.[60]

Considering the outstanding performance of tripodal molecules in chemical sensing,[61–63] we designed and synthesized a tritopic monomer (**G**) based on our previous experience, which contains a triethylamine tripod with a TPE group at each end (Scheme 1). The tripod and TPE are connected by Schiff-base units. On this basis, strong fluorescent NPs with a large Stokes shift could be obtained by reprecipitation in aqueous media due to the AIE–ESIPT dual mechanism of **G**. In addition, by introducing acceptor (A) molecules (**NDI**) into nanoparticles to achieve FRET of **G** (donor, D), an artificial light harvesting system based on the ESIPT–AIE–FRET triple mechanism can be constructed and exhibit good antenna effects. Furthermore, due to the metal-coordination ability of Schiff-base groups, it is worth noting that both **G** and light-harvesting **G–NDI** nanoparticles exhibit good detection capabilities for Fe^{3+} and Cu^{2+}.

Experimental

Materials and methods

Chemicals were purchased from commercial suppliers. Yields were given as isolated yields. $^1H/^{13}C$ NMR spectroscopy was performed on Bruker AVANCE III spectrometers (300 MHz/400 MHz). High-resolution electrospray ionization mass spectra (HR-ESI-MS) were recorded on an Agilent Technologies 6540 UHD Accurate-Mass. DLS were measured on a Zetasizer Nano ZS ZEN3600. TEM investigations were carried out on a JEM-2100 instrument. UV-vis spectra were carried out on a Perkin Elmer Lambda 35 UV-vis spectrometer. Fluorescence was performed on an Agilent Cary Eclipse spectrofluorometer. The fluorescence lifetimes were determined using time correlated single photon counting (TCSPC) on a FLS980 instrument with a pulsed xenon lamp. Analysis of fluorescence decay curves were subjected to fit a bi-exponential decay. The instrument response function (IRF) measures the scattering of laser excitation from non-fluorescent control samples to measure the fastest possible response of the detectors. The absolute fluorescence quantum yields were measured on a FLS980 instrument with an integrating sphere.

Synthesis of G

The imine group-containing compound **G** is simply synthesized by the condensation of an aldehyde group-containing the TPE derivative **P**[60] and tris(2-aminoethyl) amine (TAEA) (Scheme 1). The final compound **G** was fully characterized by $^1H/^{13}C$ NMR and high-resolution ESI-MS (Fig. S15–S17, ESI†). To a 150 mL flask, **P** (1.00 g, 2.66 mmol), TAEA (0.13 g, 0.89 mmol) and anhydrous ethanol (70 mL) were added. The mixture was stirred at room temperature for 12 hours. After that, the obtained mixture was filtered and the solid was washed with ethanol thoroughly. The orange residue was further purified by recrystallization using dichloromethane and hexane to give the yellow solid product **G** (0.90 g, 83%). ^1H NMR (300 MHz, $CDCl_3$): δ (ppm) = 13.35 (s, 3H, Ar–O*H*), 7.87 (s, 3H, –C*H*═N–), 7.08–6.99 (m, 45H, Ar–*H*), 6.90 (d, J = 8.4 Hz, 3H, Ar–*H*), 6.83 (s, 3H, Ar–*H*), 6.59 (d, J = 8.7 Hz, 3H, Ar–*H*), 3.47(br s, 6H, –CH_2–), 2.82 (br s, 6H, –CH_2–). ^{13}C NMR (100 MHz, $CDCl_3$): δ (ppm) = 165.94, 160.15, 143.95, 143.91, 143.74, 140.43, 140.03, 135.71, 134.36, 134.20, 131.55, 131.44, 131.42, 127.98, 127.84, 127.77, 126.66, 126.52, 126.45, 118.11, 116.54, 58.58, 56.03. HR-ESI-MS: m/z calcd for $C_{87}H_{72}N_4O_3$ $[M + H]^+$ = 1221.5677, found = 1221.5620.

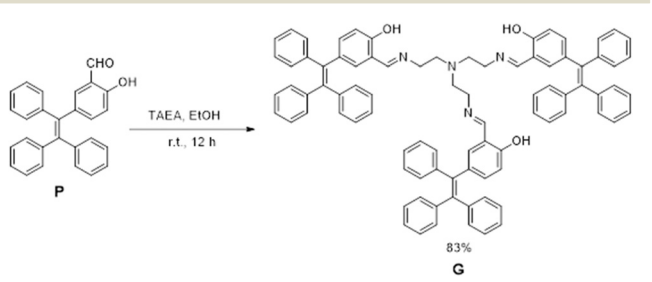

Scheme 1 Synthesis of compound **G**.

Preparation of NP dispersion

Nanoparticles of **G** are prepared by a reprecipitation method in a mixed solvent of good and poor solvents. To a tetrahydrofuran (THF) solution of **G** (5.00×10^{-4} M, 0.4 mL), deionized H_2O (3.6 mL) was added. The test concentration of **G** was kept at 50 μM. After ultrasonication at room temperature for 10 min, stable and dispersed **G** NPs in aqueous media were obtained. The nanoparticles of **G–NDI** with different D/A ratios were prepared similarly by a co-reprecipitation method.

Chemical sensing towards Fe^{3+} and Cu^{2+}

Metal cation solutions (5.00×10^{-4} M) were prepared in H_2O. Nitrate anion was used as the counter anion for all metal salts. 0.4 mL of **G** (5.00×10^{-4} M) in THF and 0.4 mL of metal cation solution were transferred into a 4 mL volumetric flask using a pipette, and then 3.2 mL of H_2O was added (f_w = 90%, [**G**] = 5.00×10^{-5} M, $[M^{n+}] = 5.00 \times 10^{-5}$ M). The test solution was ultrasonicated for 10 min. Afterwards, fluorescence testing was performed. Sensing experiments using **G–NDI** as a probe were carried out in a similar manner.

Results and discussion

Photophysical properties of G

The absorption and emission properties of **G** were first studied (Fig. S1, ESI†). The UV-vis absorption spectrum of **G** in mixed THF/H_2O (v/v = 1/9) solvent indicates the absorption maximum is at 325 nm. Interestingly, the fluorescence spectrum of **G** shows a dual emission with a weak peak at 389 nm and an intensified peak at 550 nm, which is due to the ESIPT mechanism. The weak peak at 389 nm was ascribed to the enol form of **G** (Scheme S1, ESI†). However, the excited **G** would undergo ESIPT and transform to the ketone form, resulting in a large red-shift emission at 550

nm. In the meantime, the Stokes shift of **G** was increased from 64 nm to 225 nm, which greatly avoids the self-absorption of the material.

Besides ESIPT, the AIE mechanism of **G** was further investigated. THF is a good solvent for **G**, so **G** exhibits a very weak emission in pure THF (Fig. 1a and c). Upon the addition of poor solvent H_2O into the solution, **G**'s fluorescence was remarkably increased, especially for samples with a H_2O fraction (f_w, v/v) more than 70%. The increasing trend of fluorescence intensity with f_w is shown in Fig. 1b. This should be attributed to the restriction of intramolecular movement of TPEs in **G**, which greatly reduced the non-radiation pathway. Although **G** samples with $f_w > 90\%$ exhibit a brighter fluorescence, it's not stable under this condition. Therefore, this work selects f_w = 90% as the condition to conduct all tests. The good ESIPT–AIE dual fluorescence mechanism of **G** provides a perfect prerequisite for the construction of light harvesting systems.

Morphological characterization

The morphology of the reprecipitated NPs of **G** was studied by dynamic light scattering (DLS), transmission electron microscopy (TEM) and the Tyndall effect. The DLS data of **G** showed an average hydrodynamic diameter of 263 nm (Fig. 2a), while the TEM image exhibited a regular spherical shape (Fig. 2c). The sample also shows a clear Tyndall effect, further confirming the existence of abundant NPs in aqueous solution (Fig. 2a, inset). Since **G** showed remarkable AIE emission in aqueous media, it should be a suitable candidate as the donor to fabricate man-made light harvesting NPs. The hydrophobic dye **NDI** was used as the acceptor due to the good overlap between the absorption of **NDI** and the emission of **G** (Fig. 3a). Notably, **G** has no absorption after 450 nm, ensuring the feasibility of efficient FRET. Since the tripodal structure of **G** will provide many hydrophobic microenvironmental domains in NPs, hydrophobic **NDI** can be easily trapped into NPs through co-reprecipitation. The

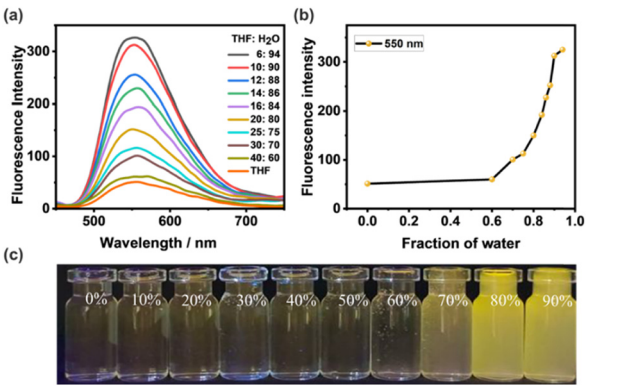

Fig. 1 (a) Fluorescence spectra of compound **G** (5.00×10^{-5} M) in THF/H_2O mixtures with different H_2O fractions, λ_{ex} = 325 nm. (b) Plot of fluorescence intensity of compound **G** at 550 nm *versus* H_2O fractions. (c) Photographs of **G** in THF/H_2O mixed solvent under UV irradiation at 365 nm.

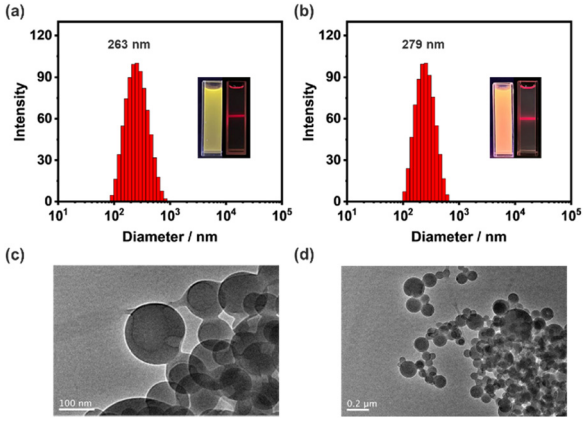

Fig. 2 DLS data of (a) **G** NPs and (b) **G–NDI** NPs. Insets: fluorescence photographs (left) of each sample and their corresponding Tyndall effects (right). TEM images of (c) **G** NPs and (d) **G–NDI** NPs. [**G**] = 5.00×10^{-5} M, [**NDI**] = 2.50×10^{-7} M, respectively.

NDI-loaded NPs were further characterized by DLS, TEM and the Tyndall effect (Fig. 2b and d), also indicative of a well-defined spherical morphology with an average hydrodynamic diameter of 279 nm.

Construction of an artificial light-harvesting system

With the **NDI**-loaded nanoparticles in hand, the energy transfer process was thoroughly studied. As shown in Fig. 3b, when **NDI** was gradually titrated into the NPs, the emission of **G** (donor, D) at 550 nm decreased obviously when excited at 325 nm. In the meantime, the emission of **NDI** (acceptor, A) at 640 nm increased significantly. Furthermore, the fluorescence color changed from yellow to red (Fig. 3c, inset).

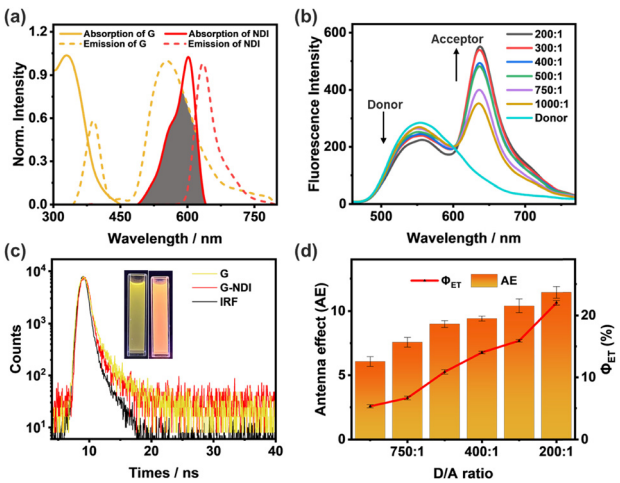

Fig. 3 (a) Normalized absorbance spectra (solid curves) of **G** (yellow trace) and **NDI** (red trace), and their normalized fluorescence spectra (dashed curves). (b) Fluorescence spectra of **G** in the presence of different concentrations of **NDI** ([**G**] = 5.00×10^{-5} M, λ_{ex} = 325 nm). (c) Fluorescence decay profiles of **G** and **G–NDI**, inset: fluorescence images of **G** (left) and **G–NDI** (right), [**G**] = 5.00×10^{-5} M, [**NDI**] = 2.50×10^{-7} M. (d) Φ_{ET} and AE at different **G**/**NDI** ratios.

These observations indicate that FRET indeed occurs from **G** to the encapsulated **NDI** molecule. The absolute fluorescence quantum yield increased from 2.76% to 5.64%, further indicating the efficient energy transfer process (Fig. S3, ESI†). In addition, this energy transfer process was further evidenced by the significant decrease in fluorescence lifetime (τ) of **G** upon the encapsulation of **NDI** (Fig. 3c). These fluorescence decay profiles were subjected to double exponential decay analysis. The fluorescence lifetimes of **G** determined at 550 nm are τ_1 = 0.76 ns and τ_2 = 3.55 ns (Table S1, ESI†). After co-assembly with 0.5% **NDI**, the fluorescence lifetimes of **G** decreased to τ_1 = 0.52 ns and τ_2 = 2.67 ns, suggesting the successful fabrication of an artificial light harvesting system.

In order to quantitatively evaluate the efficiency of these light harvesting NPs with different D/A ratios, the energy transfer efficiency (Φ_{ET}) and antenna effect (AE) were calculated according to the literature method.[18] Herein, Φ_{ET} is the ratio of the energy absorbed by **NDI** to the total excitation energy of **G**. The AE is the fluorescence amplification of **NDI** in the **G–NDI** dual-component NPs, compared to direct excitation itself. As shown in Fig. 3d, both Φ_{ET} and AE increase with the increase of **NDI**. When **G**/**NDI** reaches 200/1, the Φ_{ET} was calculated to be 22.0% (Fig. S4 and Table S3, ESI†), and the AE was 11.4 (Fig. S5 and Table S4, ESI†), indicating that the obtained **G–NDI** NPs played a good role as light-harvesting systems in aqueous media.

Fluorescence sensing for Fe^{3+} and Cu^{2+}

Since the Schiff base group has the ability to bind metal ions,[64,65] we tried to use **G** nanoparticles and **G–NDI** binary nanoparticles to construct a two-color mode probe for sensing metal ions. Firstly, we investigated the fluorescence spectra of **G** NPs upon the addition of different cations (including Li^+, Na^+, K^+, Cs^+, Mg^{2+}, Ba^{2+}, Ca^{2+}, Fe^{3+}, Cu^{2+}, Al^{3+}, Cd^{2+}, Hg^{2+}, Zn^{2+}, NH_4^+, and Ag^+, $[M^{n+}]$ = 5.00 × 10^{-5} M) in a mixed THF/H_2O solvent (f_w = 90%). As shown in Fig. 4a, the fluorescence of **G** was quenched in the presence of Fe^{3+} or Cu^{2+}, while other cations had no significant effect on the fluorescence of **G**. Subsequently, the **G–NDI** system was further used to probe Fe^{3+} or Cu^{2+} with red emission quenching (Fig. 4b). Because Fe^{3+} or Cu^{2+} can quench the emission of **G**, the FRET processes between **G** and **NDI** were also interrupted. The fluorescence quenching effects of both **G** and **G–NDI** could also be directly observed from the fluorescence photo changes under UV irradiation (Fig. 4c). The **G** NPs displayed a yellow fluorescence quenching, and the **G–NDI** NPs showed a red fluorescence quenching. Therefore, fluorescence detectors based on dual-color mode for both Fe^{3+} and Cu^{2+} were obtained.

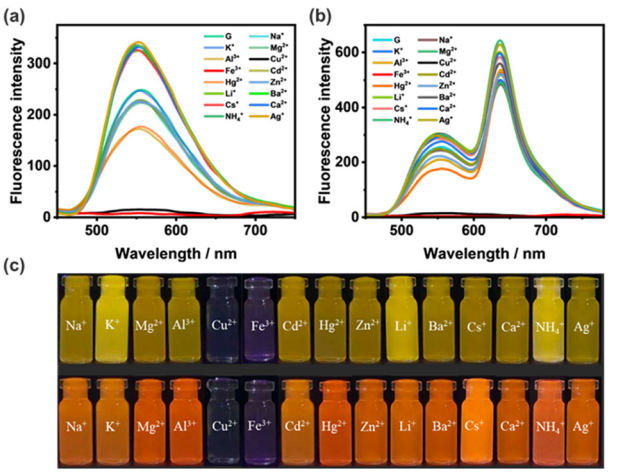

Fig. 4 (a) Fluorescence spectra of **G** NPs (5.00 × 10^{-5} M, f_w = 90%) interacting with different metal ions. (b) Fluorescence spectra of **G–NDI** NPs ([**G**] = 5.00 × 10^{-5} M, **G**/**NDI** = 200/1, f_w = 90%) interacting with different metal ions. $[M^{n+}]$ = 5.00 × 10^{-5} M, λ_{ex} = 325 nm. (c) Photograph of compound **G** (upper) and **G–NDI** (down) interacting with metal ions under a 365 nm UV lamp.

It is worth noting that both iron or copper play important biological roles in the human body.[66–69] For example, iron is involved in many metabolic processes and copper is crucial for the normal operation of the immune system. However, excessive iron or copper intake is harmful to human health. Therefore, monitoring iron or copper ions in the water environment is significantly important. Subsequently, more detailed testing on probing Fe^{3+} and Cu^{2+} was carried out. The binding behaviors of **G** with Fe^{3+} and Cu^{2+} was further evidenced by ^{1}H NMR (Fig. S6 and S7, ESI†). Upon the titration of Fe^{3+} or Cu^{2+}, the proton signal (H_a) from the hydroxyl group of **G** gradually disappeared, indicative of the coordination between metal and oxygen atoms. Notably, for Fe^{3+} and Cu^{2+} sensing, there is a dramatic difference in color change under natural light: Fe^{3+}caused a light red change, while Cu^{2+} showed no obvious color change (Fig. S8, ESI†). By selecting cations and anions as potential interfering coexisting ions, anti-interference experiments were conducted, indicating that **G** exhibits high selectivity and specific recognition for Fe^{3+} and Cu^{2+} ions (Fig. S9 and S10, ESI†). In the titration experiments of Fe^{3+} or Cu^{2+}, the fluorescence intensity of **G** gradually decreased at 550 nm, which showed a good linear relationship with the concentration of Fe^{3+} or Cu^{2+} (Fig. S11 and S12, ESI†). In addition, the fluorescence limit of detection (LOD) of **G** were calculated as 4.35 × 10^{-7} M for Fe^{3+} and 5.10 × 10^{-7} M for Cu^{2+}, which are comparable to those reported in the literature.[70–73] Furthermore, the Job's plot for **G** with Fe^{3+} and Cu^{2+} were depicted. The Job's plot of **G** and Cu^{2+} showed a stoichiometry of 1 : 1 (Fig. S13, ESI†). The Job's plot of **G** and Fe^{3+} showed a stoichiometry of 2 : 1 (Fig. S14, ESI†). Therefore, possible binding models were proposed as shown in Fig. S13c and S14c (ESI†).

In order to get further insight and evaluate the potential application of the probe **G** for detecting Fe^{3+} or Cu^{2+} in environmental water, water samples were collected from tap water, river water, and tea water, which were filtered for further testing. For either Cu^{2+} or Fe^{3+}, the fluorescence intensity of the probe **G** showed a significant fluorescence quenching at 550 nm. The recoveries were calculated in the

range of 93–103% in tap water, 100–110% in river water, and 91–99% in tea water, for Cu^{2+} (Table S5†). The recoveries were calculated in the range 97–108% in tap water, 92–106% in river water, and 99–109% in tea water, for Fe^{3+} (Table S6†). Therefore, the high selectivity and specificity of the probe **G** indicates that it could be used for monitoring Fe^{3+} or Cu^{2+} in a water environment.

Conclusions

In summary, we designed and synthesized a tripodal sensor **G**, which contains both TPE groups and Schiff base groups, ensuring the ESIPT and AIE mechanisms during the luminescence process. The **G** molecules can form nanoparticles in THF/H_2O mixed solvent (f_w = 90%) through the reprecipitation method. The nanoparticles were thoroughly characterized by the Tyndall effect, DLS, and TEM. By co-precipitation with an acceptor dye **NDI**, efficient artificial light harvesting nanoparticles could be prepared. At a high donor/acceptor ratio (D/A = 200/1), the antenna effect can reach 11.4 and the energy transfer efficiency can reach 22.0%. Moreover, both **G** nanoparticles and **G–NDI** light-harvesting nanoparticles show good Fe^{3+} and Cu^{2+} sensing abilities with dual-color fluorescence quenching phenomena. This work demonstrates a simple and green approach for constructing artificial light-harvesting system with ion-sensing ability, which may have great potential in the field of chemical probing and bioimaging.

Author contributions

Zhiying Wu: investigation, methodology, data curation, validation and writing – original draft. Qiaona Zhang: data curation and investigation. Dengli Chen: investigation. Tangxin Xiao: conceptualization, writing – original draft, preparation, project administration and supervision.

Conflicts of interest

The authors declare that they have no competing interests.

Acknowledgements

The authors are grateful for the financial support from the National Natural Science Foundation of China (21702020). D. C. acknowledges the Postgraduate Research & Practice Innovation Program of Jiangsu Province (grant no. KYCX23_3109).

References

1 R. J. Sension, *Nature*, 2007, **446**, 740–741.
2 D. Gust and T. A. Moore, *Science*, 1989, **244**, 35–41.
3 Z. Wu, H. Qian, X. Li, T. Xiao and L. Wang, *Chin. Chem. Lett.*, 2024, **35**, 108829.
4 X. M. Chen, X. Chen, X. F. Hou, S. Zhang, D. Chen and Q. Li, *Nanoscale Adv.*, 2023, **5**, 1830–1852.
5 Y. Han, X. Zhang, Z. Ge, Z. Gao, R. Liao and F. Wang, *Nat. Commun.*, 2022, **13**, 3546.
6 X. H. Wang, X. Y. Lou, T. Lu, C. Wang, J. Tang, F. Liu, Y. Wang and Y. W. Yang, *ACS Appl. Mater. Interfaces*, 2021, **13**, 4593–4604.
7 K. Wang, K. Velmurugan, B. Li and X. Y. Hu, *Chem. Commun.*, 2021, **57**, 13641–13654.
8 Y.-X. Hu, W.-J. Li, P.-P. Jia, X.-Q. Wang, L. Xu and H.-B. Yang, *Adv. Opt. Mater.*, 2020, **8**, 2000265.
9 J. Otsuki, *J. Mater. Chem. A*, 2018, **6**, 6710–6753.
10 T. Xiao, D. Chen, H. Qian, Y. Shen, L. Zhang, Z.-Y. Li and X.-Q. Sun, *Dyes Pigm.*, 2023, **210**, 110958.
11 Y. Wang, C. Q. Ma, X. L. Li, R. Z. Dong, H. Liu, R. Z. Wang, S. S. Yu and L. B. Xing, *J. Mater. Chem. A*, 2023, **11**, 2627–2633.
12 K. Wang, Y. Shen, P. Jeyakkumar, Y. Zhang, L. Chu, R. Zhang and X.-Y. Hu, *Curr. Opin. Green Sustainable Chem.*, 2023, **41**, 100823.
13 G. Sun, M. Li, L. Cai, D. Wang, Y. Cui, Y. Hu, T. Sun, J. Zhu and Y. Tang, *J. Colloid Interface Sci.*, 2023, **641**, 803–811.
14 Y. Qin, Q.-H. Ling, Y.-T. Wang, Y.-X. Hu, L. Hu, X. Zhao, D. Wang, H.-B. Yang, L. Xu and B. Z. Tang, *Angew. Chem., Int. Ed.*, 2023, **62**, e202308210.
15 J. Yu, H. Wang and Y. Liu, *Adv. Opt. Mater.*, 2022, **10**, 2201761.
16 Y. Li, C. Xia, R. Tian, L. Zhao, J. Hou, J. Wang, Q. Luo, J. Xu, L. Wang, C. Hou, B. Yang, H. Sun and J. Liu, *ACS Nano*, 2022, **16**, 8012–8021.
17 D. Zhang, W. Yu, S. Li, Y. Xia, X. Li, Y. Li and T. Yi, *J. Am. Chem. Soc.*, 2021, **143**, 1313–1317.
18 M. Hao, G. Sun, M. Zuo, Z. Xu, Y. Chen, X. Y. Hu and L. Wang, *Angew. Chem., Int. Ed.*, 2020, **59**, 10095–10100.
19 Z. Zhang, Z. Zhao, Y. Hou, H. Wang, X. Li, G. He and M. Zhang, *Angew. Chem., Int. Ed.*, 2019, **58**, 8862–8866.
20 Q. Liu, M. Zuo, K. Wang and X.-Y. Hu, *Chem. Commun.*, 2023, **59**, 13707–13710.
21 P. Jia, Y. Hu, Z. Zeng, Y. Wang, B. Song, Y. Jiang, H. Sun, M. Wang, W. Qiu and L. Xu, *Chin. Chem. Lett.*, 2023, **34**, 107511.
22 K. Wang, X. Tian, J. H. Jordan, K. Velmurugan, L. Wang and X.-Y. Hu, *Chin. Chem. Lett.*, 2022, **33**, 89–96.
23 G. Sun, M. Zuo, W. Qian, J. Jiao, X.-Y. Hu and L. Wang, *Green Synth. Catal.*, 2021, **2**, 32–37.
24 G. Sun, L. Cai, Y. Zhang, Y. Hu, J. Zhu, T. Sun and Y. Tang, *Dyes Pigm.*, 2022, **205**, 110577.
25 M. Huo, X. Y. Dai and Y. Liu, *Adv. Sci.*, 2022, **9**, e2201523.
26 X. M. Chen, Q. Cao, H. K. Bisoyi, M. Wang, H. Yang and Q. Li, *Angew. Chem., Int. Ed.*, 2020, **59**, 10493–10497.
27 T. Xiao, L. Zhang, D. Chen, Q. Zhang, Q. Wang, Z.-Y. Li and X.-Q. Sun, *Org. Chem. Front.*, 2023, **10**, 3245–3251.
28 K. Diao, D. J. Whitaker, Z. Huang, H. Qian, D. Ren, L. Zhang, Z.-Y. Li, X.-Q. Sun, T. Xiao and L. Wang, *Chem. Commun.*, 2022, **58**, 2343–2346.
29 T. Xiao, X. Wei, H. Wu, K. Diao, Z.-Y. Li and X.-Q. Sun, *Dyes Pigm.*, 2021, **188**, 109161.
30 T. Xiao, H. Qian, X. Li, Z. Wu, Z.-Y. Li and X.-Q. Sun, *Dyes Pigm.*, 2023, **215**, 111289.

31 H. Qian, T. Xiao, R. B. P. Elmes and L. Wang, *Chin. Chem. Lett.*, 2023, **34**, 108185.
32 Z. Lian, J. He, L. Liu, Y. Fan, X. Chen and H. Jiang, *Nat. Commun.*, 2023, **14**, 2752.
33 Q. Song, S. Goia, J. Yang, S. C. L. Hall, M. Staniforth, V. G. Stavros and S. Perrier, *J. Am. Chem. Soc.*, 2021, **143**, 382–389.
34 T. Xiao, L. Tang, D. Ren, K. Diao, Z.-Y. Li and X.-Q. Sun, *Chem. – Eur. J.*, 2023, **29**, e202203463.
35 X. Li, Z. Wu, Q. Wang, Z.-Y. Li, X.-Q. Sun and T. Xiao, *ChemPlusChem*, 2023, **88**, e202300431.
36 T. Xiao, D. Ren, K. Diao, J. Wang, Z. Y. Li, X. Q. Sun and L. Wang, *Chem. – Asian J.*, 2022, **17**, e202200386.
37 T. Xiao, H. Qian, Y. Shen, C. Wei, D. Ren, L. Zhang, Z. Y. Li, L. Wang and X. Q. Sun, *Mater. Today Chem.*, 2022, **24**, 100833.
38 D. Ren, L. Tang, Z. Wu, Q. Zhang, T. Xiao, R. B. P. Elmes and L. Wang, *Chin. Chem. Lett.*, 2023, **34**, 108617.
39 T. Xiao, L. Zhang, H. Wu, H. Qian, D. Ren, Z.-Y. Li and X.-Q. Sun, *Chem. Commun.*, 2021, **57**, 5782–5785.
40 T. Xiao, Y. Shen, C. Bao, K. Diao, D. Ren, H. Qian and L. Zhang, *RSC Adv.*, 2021, **11**, 30041–30045.
41 T. Xiao, H. Wu, G. Sun, K. Diao, X. Wei, Z.-Y. Li, X.-Q. Sun and L. Wang, *Chem. Commun.*, 2020, **56**, 12021–12024.
42 Y. Zhu, L. Xu, L. Wang, H. Tang and D. Cao, *Chem. Commun.*, 2019, **55**, 5910–5913.
43 C. L. Sun, H. Q. Peng, L. Y. Niu, Y. Z. Chen, L. Z. Wu, C. H. Tung and Q. Z. Yang, *Chem. Commun.*, 2018, **54**, 1117–1120.
44 B.-K. An, S.-K. Kwon, S.-D. Jung and S. Y. Park, *J. Am. Chem. Soc.*, 2002, **124**, 14410–14415.
45 H.-B. Fu and J.-N. Yao, *J. Am. Chem. Soc.*, 2001, **123**, 1434–1439.
46 S. Guo, Y. Song, Y. He, X. Y. Hu and L. Wang, *Angew. Chem., Int. Ed.*, 2018, **57**, 3163–3167.
47 H. Q. Peng, J. F. Xu, Y. Z. Chen, L. Z. Wu, C. H. Tung and Q. Z. Yang, *Chem. Commun.*, 2014, **50**, 1334–1337.
48 K. Acharyya, S. Bhattacharyya, H. Sepehrpour, S. Chakraborty, S. Lu, B. Shi, X. Li, P. S. Mukherjee and P. J. Stang, *J. Am. Chem. Soc.*, 2019, **141**, 14565–14569.
49 M. H. Chua, H. Zhou, Q. Zhu, B. Z. Tang and J. W. Xu, *Mater. Chem. Front.*, 2021, **5**, 659–708.
50 Z. Zhao, H. Zhang, J. W. Y. Lam and B. Z. Tang, *Angew. Chem., Int. Ed.*, 2020, **59**, 9888–9907.
51 F. Würthner, *Angew. Chem., Int. Ed.*, 2020, **59**, 14192–14196.
52 Y. Hong, J. W. Y. Lam and B. Z. Tang, *Chem. Soc. Rev.*, 2011, **40**, 5361–5388.
53 J. Luo, Z. Xie, J. W. Y. Lam, L. Cheng, H. Chen, C. Qiu, H. S. Kwok, X. Zhan, Y. Liu, D. Zhu and B. Z. Tang, *Chem. Commun.*, 2001, 1740–1741.
54 A. C. Sedgwick, L. Wu, H.-H. Han, S. D. Bull, X.-P. He, T. D. James, J. L. Sessler, B. Z. Tang, H. Tian and J. Yoon, *Chem. Soc. Rev.*, 2018, **47**, 8842–8880.
55 V. S. Padalkar and S. Seki, *Chem. Soc. Rev.*, 2016, **45**, 169–202.
56 J. Wu, W. Liu, J. Ge, H. Zhang and P. Wang, *Chem. Soc. Rev.*, 2011, **40**, 3483–3495.
57 L. Xu, Z. Wang, R. Wang, L. Wang, X. He, H. Jiang, H. Tang, D. Cao and B. Z. Tang, *Angew. Chem., Int. Ed.*, 2020, **59**, 9908–9913.
58 T. Xiao, W. Zhong, L. Zhou, L. Xu, X.-Q. Sun, R. B. P. Elmes, X.-Y. Hu and L. Wang, *Chin. Chem. Lett.*, 2019, **30**, 31–36.
59 Z. Xu, S. Peng, Y. Y. Wang, J. K. Zhang, I. Lazar Alexandra and D. S. Guo, *Adv. Mater.*, 2016, **28**, 7666–7671.
60 T. Xiao, C. Bao, L. Zhang, K. Diao, D. Ren, C. Wei, Z.-Y. Li and X.-Q. Sun, *J. Mater. Chem. A*, 2022, **10**, 8528–8534.
61 J. Samanta, M. Tang, M. Zhang, R. P. Hughes, R. J. Staples and C. Ke, *J. Am. Chem. Soc.*, 2023, **145**, 21723–21728.
62 Q. Lin, X.-W. Guan, Y.-Q. Fan, J. Wang, L. Liu, J. Liu, H. Yao, Y.-M. Zhang and T.-B. Wei, *New J. Chem.*, 2019, **43**, 2030–2036.
63 B. Kuswandi, Nuriman, W. Verboom and D. N. Reinhoudt, *Sensors*, 2006, **6**, 978–1017.
64 H. Sun, Y. Jiang, J. Nie, J. Wei, B. Miao, Y. Zhao, L. Zhang and Z. Ni, *Mater. Chem. Front.*, 2021, **5**, 347–354.
65 H.-F. Xie, C.-J. Yu, Y.-L. Huang, H. Xu, Q.-L. Zhang, X.-H. Sun, X. Feng and C. Redshaw, *Mater. Chem. Front.*, 2020, **4**, 1500–1506.
66 Y. Sun, P. Sun and W. Guo, *Coord. Chem. Rev.*, 2021, **429**, 213645.
67 H. J. Lee, K. J. Korshavn, A. Kochi, J. S. Derrick and M. H. Lim, *Chem. Soc. Rev.*, 2014, **43**, 6672–6682.
68 T. Kobayashi and N. K. Nishizawa, *Plant Sci.*, 2014, **224**, 36–43.
69 E. Gaggelli, H. Kozlowski, D. Valensin and G. Valensin, *Chem. Rev.*, 2006, **106**, 1995–2044.
70 X. Zhu, Y. Duan, P. Li, H. Fan, T. Han and X. Huang, *Anal. Methods*, 2019, **11**, 642–647.
71 A. Gümrükçüoğlu, Y. Topaloğlu, A. Mermer, N. Demirbaş, A. Demirbaş, M. Ocak and Ü. Ocak, *J. Fluoresc.*, 2019, **29**, 921–931.
72 J. Tang, S. Ma, D. Zhang, Y. Liu, Y. Zhao and Y. Ye, *Sens. Actuators, B*, 2016, **236**, 109–115.
73 G. J. Park, G. R. You, Y. W. Choi and C. Kim, *Sens. Actuators, B*, 2016, **229**, 257–271.